catalysts

MDPI

Article

Natural Clay Modified with ZnO/TiO_2 to Enhance Pollutant Removal from Water

Julien G. Mahy [1,*], Marlène Huguette Tsaffo Mbognou [1,2,3], Clara Léonard [1], Nathalie Fagel [4], Emmanuel Djoufac Woumfo [2] and Stéphanie D. Lambert [1]

[1] Department of Chemical Engineering—Nanomaterials, Catalysis & Electrochemistry, University of Liège, B6a, Quartier Agora, Allée du Six Août 11, 4000 Liège, Belgium; tsaffombognou@yahoo.fr (M.H.T.M.); leonardclara1@gmail.com (C.L.); stephanie.lambert@uliege.be (S.D.L.)

[2] Laboratoire de Physico-Chimie des Matériaux Minéraux, University of Yaounde I, Yaounde 337, Cameroon; edjoufac2000@yahoo.fr

[3] Institute of Geological and Mining Research (IRGM), Ministère de la Recherche Scientifique et de L'innovation du Cameroun, Yaounde 4410, Cameroon

[4] Laboratoire Argiles, Géochimie et Environnements Sédimentaires (AGEs), Department of Geology, Faculty of Sciences, University of Liège, 4000 Liège, Belgium; nathalie.fagel@uliege.be

* Correspondence: julien.mahy@uliege.be; Tel.: +32-366-3563

Abstract: Raw clays, extracted from Bana, west Cameroon, were modified with semiconductors (TiO_2 and ZnO) in order to improve their depollution properties with the addition of photocatalytic properties. Cu^{2+} ions were also added to the clay by ionic exchange to increase the specific surface area. This insertion of Cu was confirmed by ICP-AES. The presence of TiO_2 and ZnO was confirmed by the detection of anatase and wurzite, respectively, using X-ray diffraction. The composite clays showed increased specific surface areas. The adsorption property of the raw clays was evaluated on two pollutants, i.e., fluorescein (FL) and p-nitrophenol (PNP). The experiments showed that the raw clays can adsorb FL but are not efficient for PNP. To demonstrate the photocatalytic property given by the added semiconductors, photocatalytic experiments were performed under UVA light on PNP. These experiments showed degradation up to 90% after 8 h of exposure with the best ZnO-modified clay. The proposed treatment of raw clays seems promising to treat pollutants, especially in developing countries.

Keywords: smectite; adsorption; photocatalysis; pollutant removal; environment remediation

Citation: Mahy, J.G.; Tsaffo Mbognou, M.H.; Léonard, C.; Fagel, N.; Woumfo, E.D.; Lambert, S.D. Natural Clay Modified with ZnO/TiO_2 to Enhance Pollutant Removal from Water. *Catalysts* **2022**, *12*, 148. https://doi.org/10.3390/catal12020148

Academic Editor: María Victoria López Ramón

Received: 13 December 2021
Accepted: 21 January 2022
Published: 25 January 2022

1. Introduction

The population growth, intensive industrialization, and agricultural practices that occurred in recent decades have led to an increase in environmental pollution, which is now considered a global crisis [1]. This scourge has its origins in the constant improvement in the standard of living and the strong demands of consumers. In Cameroon, for example, many cotton, pharmaceutical, fertilizer, tanning, and pesticide manufacturing industries release pollutants such as dyes, pesticides, or bacteria into the environment, leading to disturbances of aquatic fauna and constituting a risk for human health [2]. Faced with this alarming situation, the global demand for water, the most vital natural resource, is increasing [3] and at the same time, the quality of freshwater sources is declining due to the presence of emerging contaminants. Most of these contaminants escape conventional wastewater treatment offered by wastewater treatment plants. The presence of these emerging pollutants in the environment is a matter of concern for most environmental agencies in developing countries [4]. This water should be treated as part of the recycling of wastewater that can be used by low-income populations for watering vegetable crops and washing cars and clothes in order to allow these populations to have a profitable and healthy economic activity.

In order to limit the arrival of these various types of refractory contaminants into the environment, effective and ecological treatment strategies have been developed, such as the use of local clays widely available in Cameroon from kaolinites, andosols, illites, and smectites [5], and globally, the use of adsorption as an efficient process to remove pollutants [6]. Clays have been the subject of different characterizations and applications [7]. For nearly three decades, many research works have been carried out on clay materials from Cameroon and their applications [8]. The search for new deposits and the characterization and valuation of clay materials are still relevant today.

Advanced oxidation processes (AOPs) have been applied in several sectors for the treatment of surface and groundwater [9,10] and for the elimination of odors and volatile organic compounds [11], as well as for water discoloration, the degradation of phytosanitary and pharmaceutical products [12], the production of molecules such as H_2 [13], and water disinfection [14]. AOPs can be used either as an oxidative pretreatment leading to easily biodegradable compounds, or as a tertiary treatment method for the removal or complete mineralization of residual pollutants [15]. This process is based on the generation of radical species able to degrade organic pollutants thanks to the use of a photocatalyst material activated by UV radiation [16]. The most-used UV-sensitive photocatalysts are TiO_2 and ZnO [17–19]. Different composites of photocatalysts have already been developed for pollutant removal [20–24].

In this work, a combination of adsorption and photocatalysis through the synthesis of mixed materials based on smectite-TiO_2 or smectite-ZnO is presented. Two types of pollutants are explored, one dye and one pesticide-type pollutant: fluorescein (FL) and p-nitrophenol (PNP), respectively. The physico-chemical properties of the pure and mixed materials are determined as well as their adsorption and photocatalytic activities. The production of mixed materials allows the use of a material already present in Cameroon and the addition of small fraction (<30%) of photocatalysts to increase the pollutant removal efficiency of the clay. The efficiency of the process and the cost can be studied and compared to other known methods.

The advantages of using semiconductor-modified clay materials for pollutant removal in water in developing countries are numerous: (i) the materials are composed primarily of natural material (the clay) directly located in the country where the pollution will be treated; (ii) the semiconductor material loading stays low (<30 wt %), reducing the cost of production; (iii) ZnO and TiO_2 are the most common semiconductor materials and can be produced with green synthesis with low use of organic reagents; (iv) the composite material presents both high adsorption capacity and photocatalytic properties, increasing its depollution properties compared to bare materials; and (v) the process for the production of the composite materials is simple.

2. Results and Discussion

2.1. Composition

Macroscopically, the raw clays, the Cu^{2+}-modified clays, and the TiO_2-modified clays are pale yellow. The ZnO-modified clays are slightly gray. The main compositions of the six different clay samples, determined by ICP-AES, are presented in Table 1.

The clays contain 9–21% of Si, 5–11% of Al, and 1–4% of Fe with an atomic Si/Al ratio equal to 2, consistent with a smectic composition [25]. The amount of copper increases up to 0.8% in the Cu^{2+}-modified samples (Table 1). The percentage of ZnO reaches 28.1% and 30.3% in the Clay/ZnO and Clay/ZnO/Cu^{2+} samples, respectively. The percentage of TiO_2 is 28.8% and 27.6% in the Clay/TiO_2 and Clay/TiO_2/Cu^{2+} samples, respectively.

The XRD patterns of the eight samples (Figure 1) allow us to estimate the crystallinity of the samples.

Table 1. Sample compositions by ICP-AES.

	Al	Si	Fe	Cu	TiO_2	ZnO
	wt %	wt %	wt %	wt %	wt %	wt %
Bare Clay	10.1	20.9	3.7	<0.1	<0.1	<0.1
Clay/Cu^{2+}	11.5	21.2	4.2	0.8	<0.1	<0.1
Clay/ZnO	5.2	9.2	1.6	<0.1	<0.1	28.1
Clay/ZnO/Cu^{2+}	6.4	11.6	1.8	0.4	<0.1	30.3
Clay/TiO_2	5.7	10.2	1.6	<0.01	28.8	<0.1
Clay/TiO_2/Cu^{2+}	5.9	11.6	1.2	0.3	27.6	<0.1

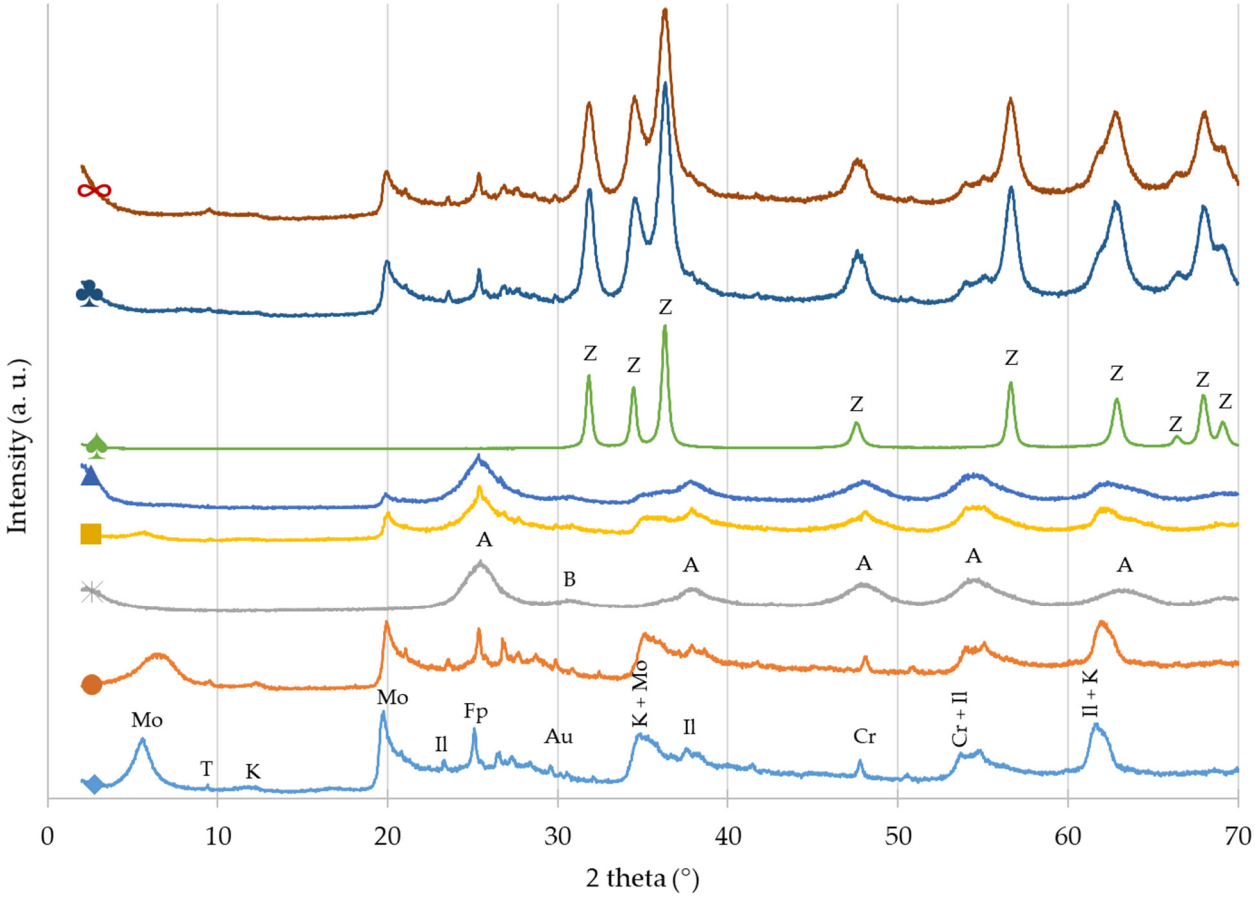

Figure 1. XRD patterns of samples: (♦) Bare Clay, (•) Clay/Cu^{2+}, (*) pure TiO_2, (■) Clay/TiO_2, (▲) Clay/TiO_2/Cu^{2+}, (♠) pure ZnO, (♣) Clay/ZnO, (∞) Clay/ZnO/Cu^{2+}. The positions of the reference peaks are indicated on the three pure materials (Bare Clay, TiO_2, and ZnO) by the following letters: (A) anatase, (B) brookite, (Z) wurzite, (Mo) montmorillonite, (T) talc, (K) kaolinite, (Il) illite, (Fp) feldspar, (Au) augite, and (Cr) cristobalite. The positions are not indicated on the composites materials to not overload the figure.

The Bare Clay (♦) is mainly composed of smectite, which is a family of different clay minerals observed in Figure 1 (all the following phases are observed: augite, cristobalite, montmorillonite, illite, kaolinite, feldspar, and talc). Smectite forms an important group of the phyllosilicate family of minerals, which are distinguished by layered structures composed of polymeric sheets of SiO_4 tetrahedra linked to sheets of (Al, Mg, Fe) $(O,OH)_6$ octahedra (Figure 2) [26–28].

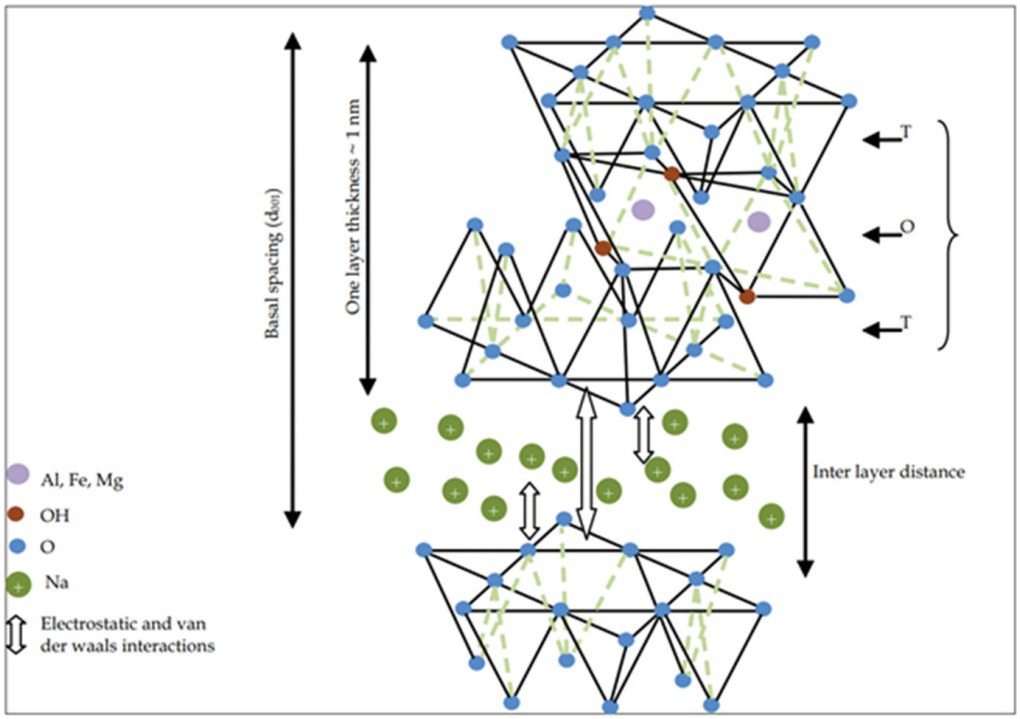

Figure 2. Smectite structure scheme from [26].

When Cu^{2+} ions are introduced to the network (Clay/Cu^{2+} sample, in orange (●) in Figure 1), a similar XRD pattern was recorded; however, the peak around 5–6° was spread due to the Cu^{2+} insertion.

The pure TiO_2 sample (Figure 1, pattern in gray (*)) is composed of anatase with a small amount of brookite (denoted A and B in Figure 1). These mixed phases were previously observed in aqueous sol-gel synthesis [29]. The pure ZnO sample (Figure 1, pattern in green (♠)) is made of wurtzite phase, as expected with this synthesis method [30].

The XRD results (Figure 1) confirm the successful production of hybrid clay–photocatalytic materials. Indeed, when the clay is modified with TiO_2, the corresponding XRD patterns (patterns in yellow (■) and mid blue (▲) in Figure 1) present the characteristic TiO_2 and clay peaks for both Clay/TiO_2 and Clay/TiO_2/Cu^{2+} samples if the peak positions are compared to the bare samples. The XRD patterns of the ZnO-modified clays (patterns in red (∞) and dark blue (♣) in Figure 1) likely present characteristic peaks of both wurtzite and clays.

2.2. Texture and Morphology

Table 2 presents the specific surface areas (S_{BET}) of the different samples, ranging from 30 to 325 m^2/g. The Bare Clay sample has a relatively low specific surface area (45 m^2/g), which increases slightly when Cu^{2+} ions are intercalated (55 m^2/g). This increase comes from the insertion of the cations in the smectite network [28]; indeed, this insertion is observed in the XRD patterns (Figure 1) with the spread of the peak around 5°. The pure TiO_2 sample presents an S_{BET} value equal to 180 m^2/g, in agreement with literature data [29]. When the clay is modified with TiO_2, S_{BET} increases to 325 and 240 m^2/g for Clay/TiO_2 and Clay/TiO_2/Cu^{2+} samples, respectively. This is logical, as these composite materials are produced with nanospheres of TiO_2, which have high specific surface area. They can also enter the clay network to expand the material and thus increase its specific surface area. The pure ZnO sample presents a low S_{BET} value (30 m^2/g). When clay is modified with ZnO, the specific surface area increases for Clay/ZnO sample (125 m^2/g), but it stays relatively low for Clay/ZnO/Cu^{2+} (50 m^2/g). The increased surface area of the Clay/ZnO sample could come from an insertion of some ZnO particles inside the clay network.

Table 2. Specific surface areas of samples.

Sample	Specific Surface Area (m^2/g) ± 5
Bare Clay	45
Clay/Cu^{2+}	55
Pure TiO_2	180
Clay/TiO_2	325
Clay/Cu^{2+}/TiO_2	240
Pure ZnO	30
Clay/ZnO calcine à 300 °C	125
Clay/Cu^{2+}/ZnO	50

Concerning the nitrogen adsorption–desorption isotherms, two different types are observed between all samples: (i) type I isotherm, with a sharp increase at low pressure followed by a plateau corresponding to microporous solid; and (ii) type IV isotherm, characterized by a broad hysteresis at high pressure (mesoporous solid). Samples containing TiO_2 have type I isotherms, and the other samples have type IV isotherms. As an example, the isotherms of Bare Clay and Clay/TiO_2 samples are plotted in Figure 3. The other isotherms are represented in Figures S1 and S2 in the Supplementary Materials.

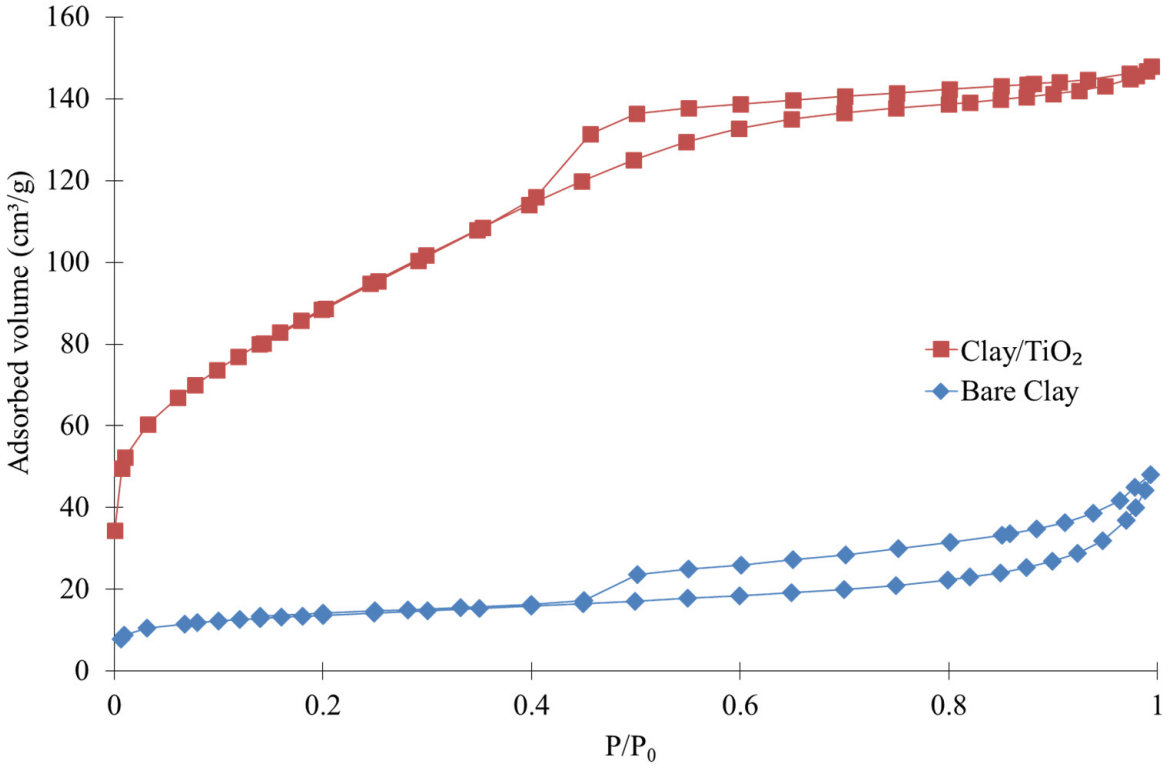

Figure 3. Nitrogen adsorption–desorption isotherms for (♦) Bare Clay and (■) Clay/TiO_2 samples.

SEM pictures of several samples are presented in Figure 4 for Bare Clay, Clay/TiO_2, and Clay/ZnO at two different magnifications. Bare Clay and Clay/ZnO samples have a similar aspect (Figure 4a,c), with large, granular powder, while the Clay/TiO_2 powder is finely dispersed (Figure 4b). These observations are in agreement with the higher specific surface area of Clay/TiO_2 and Clay/TiO_2/Cu^{2+} samples, characteristic of smaller hybrid particles and resulting in smaller voids between particles. This finely dispersed aspect comes from the TiO_2 nanoparticles, which are very small (5–10 nm), as observed in the TEM pictures of pure TiO_2 samples (Figure 5a). Contrarily, the pure ZnO sample has larger

particles (Figure 5b), indicating that the composite material with clay is more similar to the Bare Clay.

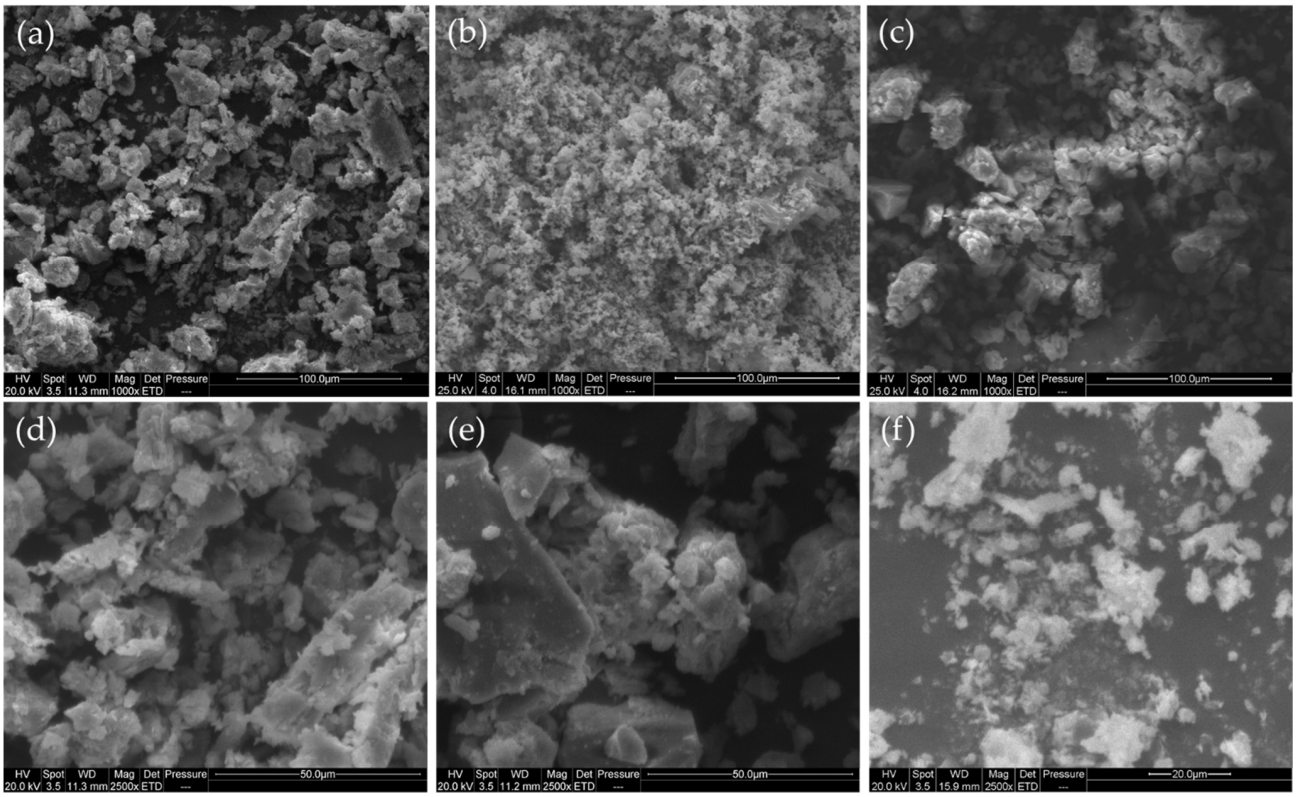

Figure 4. SEM pictures of (**a**) Bare Clay, (**b**) Clay/TiO_2, and (**c**) Clay/ZnO samples at 1000× magnification; (**d**) Bare Clay, (**e**) Clay/TiO_2, and (**f**) Clay/ZnO) at 2500× magnification.

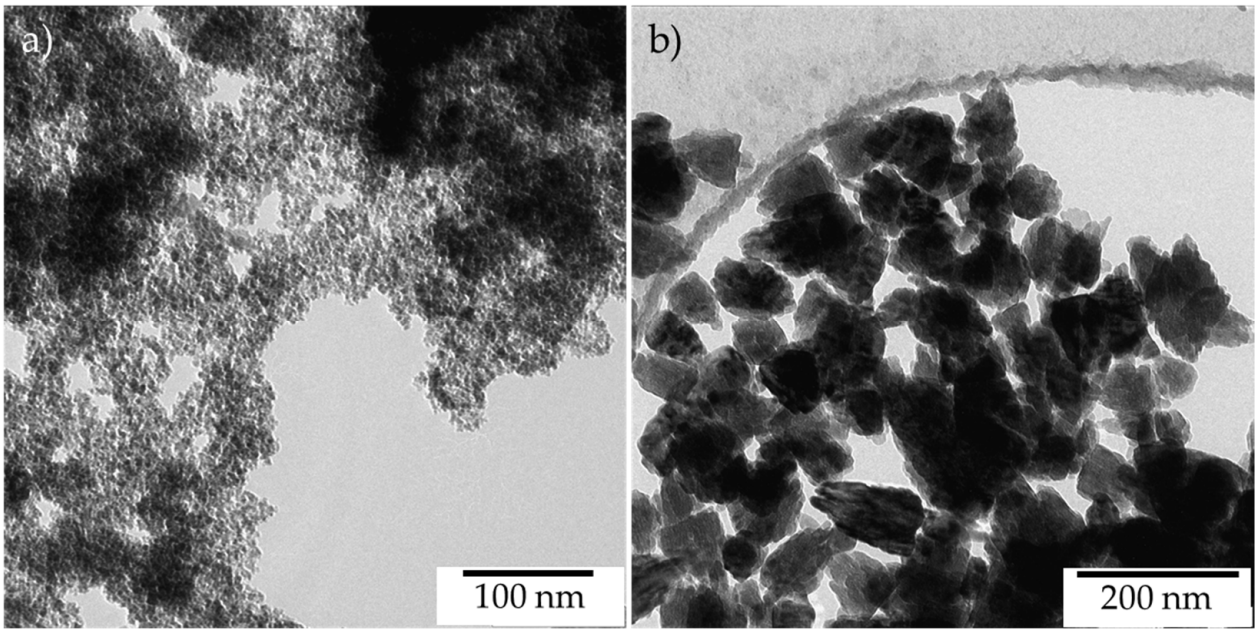

Figure 5. TEM pictures of (**a**) pure TiO_2 and (**b**) pure ZnO.

The samples with Cu^{2+} (Clay/Cu^{2+}, Clay/TiO_2/Cu^{2+} and Clay/ZnO/Cu^{2+}) have similar aspects and are represented in Supplementary Figure S3.

ICP results (Table 1) confirmed the presence of the semiconductor materials in the composite materials.

2.3. Adsorption Study

The experimental results of fluorescein adsorption are transformed with the following equation to determine the amount of FL adsorbed per g of clay (q_e):

$$q_e = \frac{(C_0 - C_e) * V}{W} \quad (1)$$

where C_0 and C_e are the initial and equilibrium liquid-phase concentrations of FL (mg_{FL} L^{-1}), respectively; V is the volume of the FL solution (L); and W is the mass of clay used (g_C).

q_e in function of C_e is represented in Figure 6a after 6 h of adsorption for Bare Clay and Clay/Cu^{2+} samples. Similar curves are obtained for both samples; indeed, they have similar specific surface areas (Table 2).

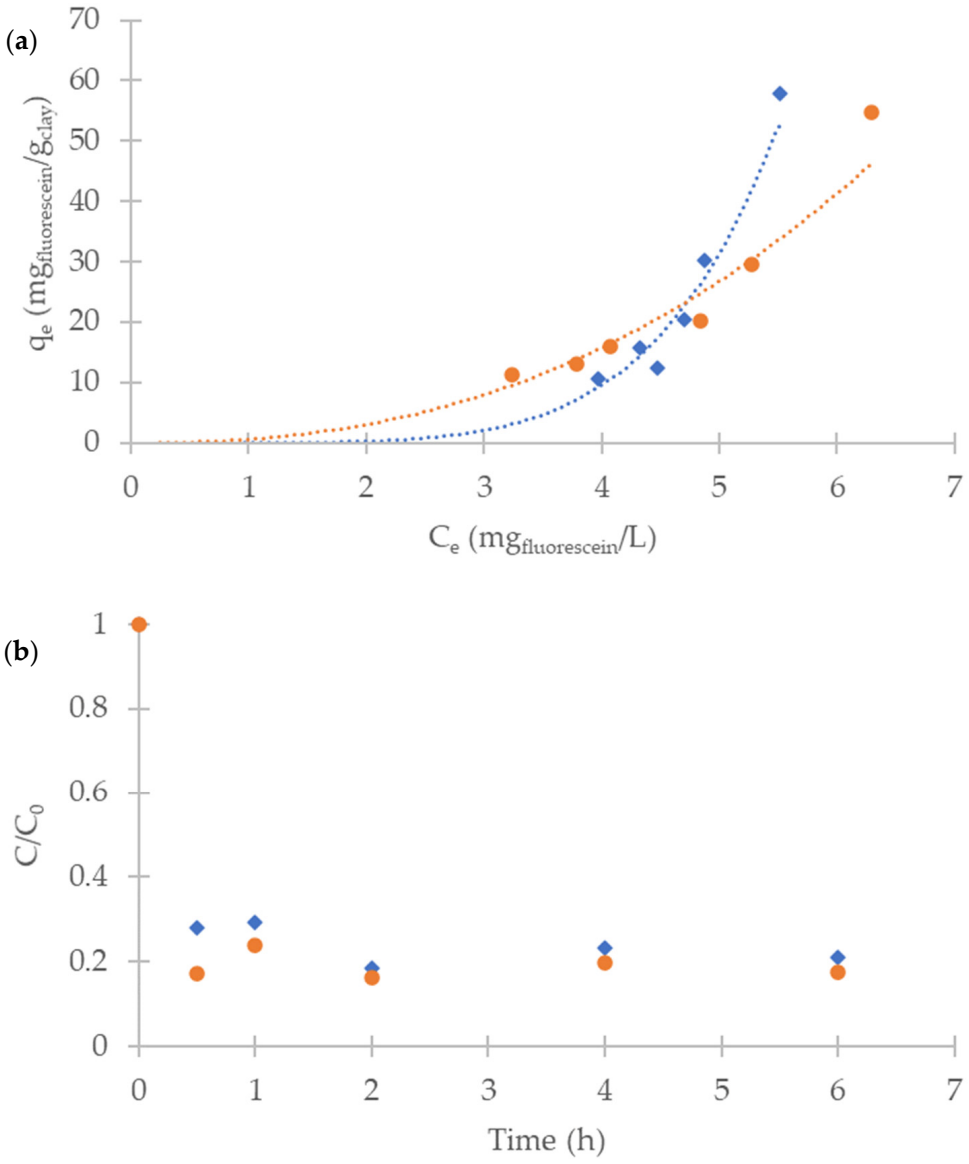

Figure 6. (**a**) Experimental fluorescein adsorption experiment representing the amount of FL adsorbed per g of clay in function of the equilibrium liquid-phase concentrations of FL after 6 h adsorption tests for the 6 different concentrations of powder samples for (♦) Bare Clay and (•) Clay/Cu^{2+} samples. (**b**) C/C_0 evolution with time for 30 mg concentrations of powder samples for (♦) Bare Clay and (•) Clay/Cu^{2+}.

In Figure 6b, the evolution of the FL concentration (C/C_0) with time is represented for Bare Clay and Clay/Cu^{2+} with 30 mg concentrations of powder samples. After 0.5 h of the experiment, more than 75% of FL were adsorbed for both samples (Figure 6b) and the concentration did not decrease much after 6 h; thus, the equilibrium was reached.

An example of the FL UV-visible spectrum is given in Figure S4 in the Supplementary Materials.

The PNP adsorption study shows that PNP is not adsorbed on the clay. Indeed, the concentration in solution remains constant with time. The removal of this kind of pollutant requires photocatalytic properties.

2.4. Photocatalytic Activity

As observed in the previous section, the clay can adsorb some pollutants such as dye, but it is not efficient to adsorb, for instance, PNP. Therefore, the clay was modified with photocatalysts to degrade molecules that cannot be efficiently adsorbed. Adsorption experiments in the dark (to avoid an interaction with room light which can activate the photocatalytic materials) were performed on all eight samples in contact with PNP for 8 h. No change in the PNP concentration was observed, showing that none of the samples adsorb the PNP molecule.

The photocatalytic property was evaluated on the PNP degradation under UVA illumination after 8 h of exposure (Figure 7a). An example of the PNP UV-visible spectrum is given in Figure S5 in the Supplementary Materials.

The Bare Clay and Clay/Cu^{2+} samples originally had no photocatalytic properties. However, such properties were attained after treatment with either TiO_2 or ZnO. PNP was degraded from 45% to 92% according to the samples. Clay/ZnO/Cu^{2+} is the most efficient material, with PNP degradation of 92%. The pure TiO_2 and ZnO materials reached 100% PNP degradation, as observed in previous studies [18,19].

For the same amount of semiconductor material (TiO_2 or ZnO), the ZnO-modified clay is more efficient than the TiO_2-modified one. As previously observed [18,31], ZnO materials have better activity than TiO_2, due to fewer recombinations of photogenerated species. The addition of Cu^{2+} ions increases the photoactivity due to an additional photo-Fenton effect that improves the PNP degradation [32]. Indeed, Cu^{2+} ions can react with water when exposed to UV radiation to produce additional $^{\bullet}OH$ radicals [32]. These radicals can degrade the organic molecules and thus enhance the photoactivity [32]. The equation of Cu^{2+} photo-Fenton effects is the following [32]:

$$Cu^{2+} + H_2O + h\nu \rightarrow Cu^{+} + {}^{\bullet}OH + H^{+}$$

where h is the Planck constant (6.63×10^{-34} J.s) and ν is the light frequency (Hz).

For the two best composite materials (Clay/TiO_2/Cu^{2+} and (•) Clay/ZnO/Cu^{2+}), the evolution of the PNP degradation over time is presented in Figure 7b. The evolution of the degradation is linear; then, the degradation is first order.

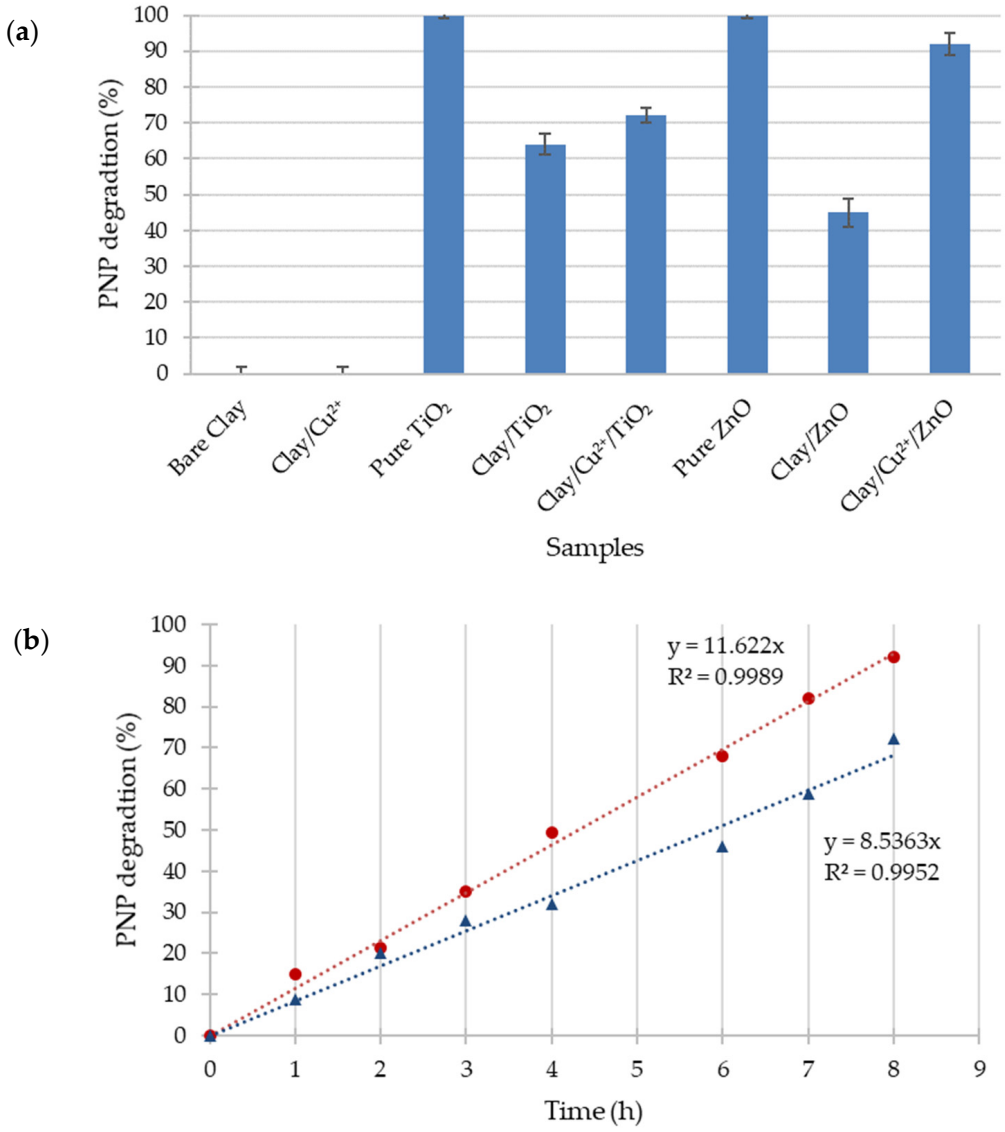

Figure 7. (**a**) PNP degradation (%) under UVA illumination for 8 h with all samples and (**b**) PNP degradation evolution over 8 h for the two best composite samples, (▲) Clay/TiO_2/Cu^{2+} and (●) Clay/ZnO/Cu^{2+}.

3. Materials and Methods

3.1. Description of the Clay and Modification with Cu^{2+} Ions

3.1.1. Presentation of the Clay

The clay material was whitish in color, sampled at 20 cm depth. The UTM coordinates of the sampling were north 5°06′08.3″ and east 10°17′28.0″, at an altitude of 1423 m. These coordinates corresponded to Mont Batcha, commonly called Bakotcha, in the district of Bana (West Cameroon). This region has an equatorial climate, characterized by average annual rainfall of 1300–2500 mm and a mean annual temperature of 21.23 °C [33]. The vegetation is highly anthropogenized post-forestry savannah with remains of a persisting semi-deciduous forest in areas of difficult accessibility [34]. The dominant soil types are red ferralitic soils, associated with brunified and hydromorphic soils [35]. The sampled clay was air-dried in the laboratory to a constant weight before grinding and sieving in a 160 µm diameter sieve.

3.1.2. Modification of Clay with Ions Cu^{2+} or Interfoliar Cation Exchange

This treatment does not destroy the structure of the clay material and it allows the insertion of ions (as shown in Figure 2). We used the following reagents: copper (II) sulfate pentahydrate (>98.0% from LabChem, Gauteng, South Africa), barium sulfate (99%, pure, from Laboratoriumdiscounter), clay powder (>160 µm), and distilled water.

In order to produce a homogeneous cation exchange, 50 g of clay was mixed under stirring in 0.1 M of $CuSO_4$ solution for 4 h. After 2 h rest, the supernatant was poured, and the agitation was repeated with a new solution of 0.1 M of $CuSO_4$. This operation was repeated twice, and excess Cu^{2+} and $SO_4{}^{2-}$ ions were washed with distilled water until the Baryum test (precipitation test) became negative. The homoionic Cu^{2+} clay material was then oven-dried at 110 °C overnight.

3.2. Synthesis of Pure TiO_2 and ZnO Photocatalysts

3.2.1. ZnO Sample

Pure zinc oxide powders were synthesized by the sol-gel method following Benhebal et al. [30,36]. The reagents were zinc acetate dihydrate (≥98%), oxalic acid dihydrate (≥99%), and absolute ethanol (ACS grade). They were obtained from BIOCHEM, Chemopharma (Cosne-Cours-sur-Loire, France), of analytical grade, and used directly as purchased.

Zinc acetate dihydrate (10.98 g) was treated with ethanol (300 mL) at 60 °C. The salt was completely dissolved in about 30 min. Oxalic acid dihydrate (12.6 g) was dissolved in ethanol (200 mL) at 60 °C for 30 min. The oxalic acid solution was added slowly, with stirring, to the hot ethanolic zinc solution, and the mixture was stirred for 90 min at 50 °C. The resulting gel was placed in an oven at 80 °C for 24 h. The product was calcined at 400 °C for 4 h. The color of the pure ZnO powder was white.

3.2.2. TiO_2 Sample

Pure titanium oxide powders were synthesized by the sol-gel method of Mahy et al. [32]. The reagents used were titanium (IV) tetraisopropoxide (TTIP > 97%, Sigma-Aldrich, St. Louis, MO, USA), nitric acid (HNO_3, 65%, Merck, Darmstadt, Germany), isopropanol (IsoP, 99.5%, Acros, Hull, Belgium), and distilled water.

Nitric acid HNO_3 (65%, Merck) was used to acidify 250 mL of distilled water to pH 1. Then, 15 mL of TTIP was added to 15 mL of isopropanol (IsoP), and the mixture was stirred for 30 min at room temperature. The resulting solution of TTIP + IsoP mixture was added to acidified water under controlled stirring. The liquid was left under stirring for 4 h at 80 °C. The obtained sol had a clear blue color. Then, the sol was dried for 10 h under an ambient air flow to obtain a xerogel. The powders were dried at 100 °C for 1 h and a pure TiO_2 powder of yellowish-white color was obtained [32].

3.3. Synthesis of Hybrid Clay/Photocatalyst Materials

3.3.1. Clay/ZnO Materials

For the preparation of modified clays with ZnO, the procedure was similar as for pure ZnO material. However, when the oxalic acid solution was added slowly with stirring to the hot ethanolic zinc solution, 10 g of clay materials was added, and the mixture was left under stirring for 90 min at 50 °C. The resulting gel was placed in an oven at 80 °C for 24 h. The product was calcined at 400 °C for 4 h. The ZnO-modified clay powders were light gray in color.

3.3.2. Clay/TiO_2 Materials

For the preparation of hybrid clay/TiO_2 powders, the same protocol of preparation of pure TiO_2 powder was used with the addition of 10 g of clay material. When the mixture TTIP + IsoP was obtained, it was added to acidified water under controlled stirring and the liquid was left under stirring for 4 h at 80 °C. To the obtained sol, clear blue in color, 10 g of clayey material was added and left under stirring for 2 h. The soil was dried for 24 h

under an ambient air flow. The powders were dried at 100 °C for 1 h and hybrid clay/TiO_2 powders were obtained.

3.4. Characterization of Samples

The actual composition of the bare and modified clays was determined by inductively coupled plasma–atomic emission spectroscopy (ICP–AES), equipped with an ICAP 6500 THERMO Scientific device (Waltham, MA, USA). The mineralization is fully described in [32]; however, we used HF instead of HNO_3.

The crystallographic properties were observed through the X-ray diffraction (XRD) patterns recorded with a Bruker D8 Twin-Twin powder diffractometer (Bruker, Billerica, MA, USA) using Cu-Kα radiation.

The specific surface area of samples was determined by nitrogen adsorption–desorption isotherms in an ASAP 2420 multi-sampler volumetric device from Micromeritics (Norcross, GA, USA) at 77 °K.

SEM micrographs were obtained using a Jeol-JSM-6360LV microscope (Tokyo, Japan) under high vacuum at an acceleration voltage of 20 kV.

Transmission electron microscopy was performed on the LEO 922 OMEGA Energy Filter Transmission Electron Microscope (Zeiss, Oberkochen, Germany) operating at 120 kV. Sample preparation consisted of dispersing a few milligrams of each sample in water, using sonication. Then, a few drops of the supernatant were placed on a holed carbon film deposited on a copper grid (CF-1.2/1.3-2 Cu-50, C-flat™, Protochips, Morrisville, NC, USA).

3.5. Adsorption Experiments

Concerning the adsorption experiments, only the Bare Clay and Clay/Cu^{2+} samples were assessed. The adsorption of two types of model pollutants, fluorescein (FL) and p-nitrophenol (PNP), was tested. For an adsorption experiment, 6 vials were prepared containing 5, 10, 15, 20, 25, and 30 mg of powder clay and 20 mL of pollutant solution in water. The samples were under continuous stirring. The remaining concentration in solution was evaluated every hour for 6 h with a Genesys 10S UV-Vis spectrophotometer (Thermo Scientific) after filtration with a syringe filter. The main absorption peaks were located at 317 and 485 nm for PNP and FL, respectively, as shown in Figures S4 and S5 in the Supplementary Materials. The initial concentration of FL was 6×10^{-5} M and 10^{-4} M for PNP.

3.6. Photocatalytic Experiments

The degradation of p-nitrophenol (PNP) was studied under UVA light (λ = 365 nm) to determine the photocatalytic activity of the synthesized material. The lamp was an Osram Sylvania, Blacklight-Bleu Lamp, F 18W/BLB-T8, considered as monochromatic at 365 nm.

Each sample was placed in a Petri dish with 20 mL of 10^{-4} M of PNP solution in water. The degradation of PNP was evaluated from absorbance measurements with a Genesys 10S UV-Vis spectrophotometer (Thermo Scientific) at λ = 317 nm. Previously, adsorption tests were performed in the dark (dark tests) to show whether PNP was adsorbed on the surface of samples. A blank test, consisting of irradiating the pollutant solution for 24 h in a Petri dish without any catalyst, showed that PNP concentration under UVA illumination remained constant. The Petri dishes with catalysts and pollutants were stirred on orbital shakers and illuminated for 8 h. Aliquots of PNP were sampled at 0, 4, and 8 h. The photocatalytic degradation was equal to the total degradation of PNP, taking the catalyst adsorption (dark test) into account. Each photocatalytic measurement was triplicated to assess the reproducibility of the data. In each box, the catalyst concentration was 1 g/L.

4. Conclusions

In this work, natural clays were used to remove pollutants from water by adsorption and photocatalysis processes. The approach was applied on smectite-rich Cameroon clays.

The clays were preliminarily treated with Cu^{2+} and then with semiconductors TiO_2 and ZnO to produce hybrid clays. The aim was to increase the depollution efficiency of these modified clayey materials by their photocatalytic properties. The protocol was controlled by XRD and ICP-AES measurements. The modified clays displayed an increase in their specific surface areas in comparison with natural clay properties. XRD confirmed the presence of crystalline TiO_2 and ZnO.

The adsorption experiments confirmed the bare clays can adsorb fluorescein, but they were not efficient on other pollutants, namely p-nitrophenol. The addition of semiconductor materials improved the degradation of the pollutants when exposed to UVA light. Photocatalytic experiments on PNP gave degradation levels of 70% to 90% after 8 h of exposition with the TiO_2- and ZnO-modified clays, respectively.

This study emphasizes the importance of composite clays to remove pollutants via adsorption and photocatalysis processes. Such approaches offer an opportunity, especially in developing countries, to use natural clay materials with slight modifications for water purification.

Supplementary Materials: The following are available online at https://www.mdpi.com/article/10.3390/catal12020148/s1, Figure S1: Nitrogen adsorption desorption isotherms for (♦) pure TiO_2 and (■) pure ZnO samples, Figure S2: Nitrogen adsorption desorption isotherms for (♦) Clay/Cu^{2+}, (▲) Clay/TiO_2/Cu^{2+}, (×) Clay/ZnO/Cu^{2+} and (■) Clay/ZnO samples, Figure S3: SEM pictures of (a) Clay/Cu^{2+}, (b) Clay/TiO_2/Cu^{2+} and (c) Clay/ZnO/Cu^{2+} samples at a 1000x magnification, Figure S4: FL UV/visible spectrum for (•) initial FL solution and (▲) after 6 h in adsorption experiment with bare Clay sample; Figure S5: PNP UV/visible spectrum for (•) initial PNP solution and (■) after 8 h in photocatalytic experiment with Clay/TiO_2 sample.

Author Contributions: Conceptualization, methodology, investigation, analysis, and writing, J.G.M., M.H.T.M. and S.D.L.; writing—original draft preparation, J.G.M., M.H.T.M. and S.D.L.; XRD characterizations analysis, M.H.T.M. and N.F.; adsorption experiments, J.G.M. and C.L.; supervision, funding acquisition, and project administration, E.D.W. and S.D.L. All the authors corrected the paper before submission and during the revision process. All authors have read and agreed to the published version of the manuscript.

Funding: This research was funded by PACODEL/University of Liège, bourse de mobilité doctorale.

Data Availability Statement: The raw/processed data required to reproduce these findings cannot be shared at this time as these data are part of an ongoing study.

Acknowledgments: J.G.M. and S.D.L. thank the Belgian National Funds for Scientific Research (F.R.S.-FNRS) for his postdoctoral fellowship and her senior associate researcher position, respectively. The authors thank the CARPOR platform of the University of Liège and its manager, Alexandre Léonard, for the nitrogen adsorption–desorption measurements.

Conflicts of Interest: The authors declare no conflict of interest.

References

1. Kemgang Lekomo, Y.; Mwebi Ekengoue, C.; Douola, A.; Fotie Lele, R.; Christian Suh, G.; Obiri, S.; Kagou Dongmo, A. Assessing Impacts of Sand Mining on Water Quality in Toutsang Locality and Design of Waste Water Purification System. *Clean. Eng. Technol.* **2021**, *2*, 100045. [CrossRef]
2. Auriol, M.; Filali-Meknassi, Y.; Dayal Tyagi, R. Présence et Devenir Des Hormones Stéroïdiennes Dans Les Stations de Traitement Des Eaux Usées. Occurrence and Fate of Steroid Hormones in Wastewater Treatment Plants. *Rev. Des Sci. L'eau* **2007**, *20*, 89–108.
3. Ekengoue, C.M.; Lele, R.F.; Dongmo, A.K. Influence De L'exploitation Artisanale Du Sable Sur La Santé Et La Sécurité Des Artisans Et L'environnement: Cas De La Carrière De Nkol'Ossananga, Région Du Centre Cameroun. *Eur. Sci. J. ESJ* **2018**, *14*, 246. [CrossRef]
4. Available online: Https://Minepded.Gov.Cm/Fr/ (accessed on 18 November 2021).
5. Nkoumbou, C.; Njopwouo, D.; Villiéras, F.; Njoya, A.; Yonta Ngouné, C.; Ngo Ndjock, L.; Tchoua, F.M.; Yvon, J. Talc Indices from Boumnyebel (Central Cameroon), Physico-Chemical Characteristics and Geochemistry. *J. Afr. Earth Sci.* **2006**, *45*, 61–73. [CrossRef]

6. Filice, S.; Bongiorno, C.; Libertino, S.; Compagnini, G.; Gradon, L.; Iannazzo, D.; la Magna, A.; Scalese, S. Structural Characterization and Adsorption Properties of Dunino Raw Halloysite Mineral for Dye Removal from Water. *Materials* **2021**, *14*, 3676. [CrossRef]
7. Jacques Richard, M. *Mineralogie et Proprietes Physico-Chimiques des Smectites de Bana et Sabga (Cameroun). Utilisation Dans La Décoloration d' Une Huile Végétale Alimentaire*; Université de Liège: Liège, Belgique, 2013.
8. Djoufac Woumfo, E.; Elimbi, A.; Panczer, G.; Nyada Nyada, R.; Njopwouo, D. Physico-Chemical and Mineralogical Characterization of Garoua Vertisols (North Cameroon). *Ann. Chim.* **2006**, *31*, 75–90.
9. Léonard, G.L.-M.; Malengreaux, C.M.; Mélotte, Q.; Lambert, S.D.; Bruneel, E.; van Driessche, I.; Heinrichs, B. Doped Sol–Gel Films vs. Powders TiO_2: On the Positive Effect Induced by the Presence of a Substrate. *J. Environ. Chem. Eng.* **2016**, *4*, 449–459. [CrossRef]
10. Parsons, S. *Advanced Oxidation Processes for Water and Wastewater Treatment*; IWA Publishing: London, UK, 2004; ISBN 1843390175.
11. Bhowmick, M.; Semmens, M.J. Ultraviolet Photooxidation for the Destruction f VOCs in Air. *Wat. Res.* **1994**, *28*, 2407–2415. [CrossRef]
12. Ikehata, K.; El-Din, M.G. Aqueous Pesticide Degradation by Hydrogen Peroxide/Ultraviolet Irradiation and Fenton-Type Advanced Oxidation Processes: A Review. *J. Environ. Eng. Sci.* **2006**, *5*, 81–135. [CrossRef]
13. Filice, S.; Fiorenza, R.; Reitano, R.; Scalese, S.; Sciré, S.; Fisicaro, G.; Deretzis, I.; la Magna, A.; Bongiorno, C.; Compagnini, G. TiO2 Colloids Laser-Treated in Ethanol for Photocatalytic H2 Production. *ACS Appl. Nano Mater.* **2020**, *3*, 9127–9140. [CrossRef]
14. Goncharuk, V.V.; Potapchenko, N.G.; Savluk, O.S.; Kosinova, V.N.; Sova, A.N. Study of Various Conditions for O3/UV Disinfection of Water. *Khimiya Tecknol. Vody* **2003**, *25*, 487–496.
15. Drogui, P.; Blais, J.-F.; Mercier, G. Review of Electrochemical Technologies for Environmental Applications. *Recent Pat. Eng.* **2007**, *1*, 257–272. [CrossRef]
16. Douven, S.; Mahy, J.G.; Wolfs, C.; Reyserhove, C.; Poelman, D.; Devred, F.; Gaigneaux, E.M.; Lambert, S.D. Efficient N, Fe Co-Doped TiO_2 Active under Cost-Effective Visible LED Light: From Powders to Films. *Catalysts* **2020**, *10*, 547. [CrossRef]
17. Mahy, J.G.; Wolfs, C.; Vreuls, C.; Drot, S.; Dircks, S.; Boergers, A.; Tuerk, J.; Hermans, S.; Lambert, S.D. Advanced Oxidation Processes for Waste Water Treatment: From Lab-Scale Model Water to on-Site Real Waste Water. *Environ. Technol.* **2021**, *42*, 3974–3986. [CrossRef] [PubMed]
18. Mahy, J.G.; Lejeune, L.; Haynes, T.; Body, N.; de Kreijger, S.; Elias, B.; Marcilli, R.H.M.; Fustin, C.A.; Hermans, S. Crystalline ZnO Photocatalysts Prepared at Ambient Temperature: Influence of Morphology on p-Nitrophenol Degradation in Water. *Catalysts* **2021**, *11*, 1182. [CrossRef]
19. Bodson, C.J.; Heinrichs, B.; Tasseroul, L.; Bied, C.; Mahy, J.G.; Man, M.W.C.; Lambert, S.D. Efficient P- and Ag-Doped Titania for the Photocatalytic Degradation of Waste Water Organic Pollutants. *J. Alloys Compd.* **2016**, *682*, 144–153. [CrossRef]
20. Cheng, T.; Gao, H.; Liu, G.; Pu, Z.; Wang, S.; Yi, Z.; Wu, X.; Yang, H. Preparation of Core-Shell Heterojunction Photocatalysts by Coating CdS Nanoparticles onto Bi4Ti3O12 Hierarchical Microspheres and Their Photocatalytic Removal of Organic Pollutants and Cr(VI) Ions. *Colloids Surf. A Physicochem. Eng. Asp.* **2022**, *633*, 127918. [CrossRef]
21. Xiong, S.; Yin, Z.; Zhou, Y.; Peng, X.; Yan, W.; Liu, Z.; Zhang, X. The Dual-Frequency (20/40 KHz) Ultrasound Assisted Photocatalysis with the Active Carbon Fiber-Loaded Fe3+-TiO2 as Photocatalyst for Degradation of Organic Dye. *Bull. Korean Chem. Soc.* **2013**, *34*, 3039–3045. [CrossRef]
22. Li, Y.; Li, M.; Xu, P.; Tang, S.; Liu, C. Efficient Photocatalytic Degradation of Acid Orange 7 over N-Doped Ordered Mesoporous Titania on Carbon Fibers under Visible-Light Irradiation Based on Three Synergistic Effects. *Appl. Catal. A Gen.* **2016**, *524*, 163–172. [CrossRef]
23. Tang, N.; Li, Y.; Chen, F.; Han, Z. In Situ Fabrication of a Direct Z-Scheme Photocatalyst by Immobilizing CdS Quantum Dots in the Channels of Graphene-Hybridized and Supported Mesoporous Titanium Nanocrystals for High Photocatalytic Performance under Visible Light. *RSC Adv.* **2018**, *8*, 42233–42245. [CrossRef]
24. Lin, X.; Li, M.; Li, Y.; Chen, W. Enhancement of the Catalytic Activity of Ordered Mesoporous TiO_2 by Using Carbon Fiber Support and Appropriate Evaluation of Synergy between Surface Adsorption and Photocatalysis by Langmuir-Hinshelwood (L-H) Integration Equation. *RSC Adv.* **2015**, *5*, 105227–105238. [CrossRef]
25. Ndé, H.S.; Tamfuh, P.A.; Clet, G.; Vieillard, J.; Mbognou, M.T.; Woumfo, E.D. Comparison of HCl and H_2SO_4 for the Acid Activation of a Cameroonian Smectite Soil Clay: Palm Oil Discolouration and Landfill Leachate Treatment. *Heliyon* **2019**, *5*, e02926. [CrossRef] [PubMed]
26. Olad, A. 7 Polymer/Clay Nanocomposites. In *Advances in Diverse Industrial Applications of Nanocomposites*; Reddy, B., Ed.; InTechOpen: London, UK, 2011.
27. Yeop Lee, S.; Jin Kim, S. Expansion of smectite by hexadecyltrimethylammonium. *Clays Clay Miner.* **2002**, *50*, 435–445.
28. Theo Kloprogge, J.; Komarnenl, S.; Amonetie, J.E. Synthesis of smectite clay minerals: A critical review. *Clays Clay Miner.* **1999**, *47*, 529–554. [CrossRef]
29. Mahy, J.G.; Léonard, G.L.-M.; Pirard, S.; Wicky, D.; Daniel, A.; Archambeau, C.; Liquet, D.; Heinrichs, B. Aqueous Sol-Gel Synthesis and Film Deposition Methods for the Large-Scale Manufacture of Coated Steel with Self-Cleaning Properties. *J. Sol-Gel Sci. Technol.* **2017**, *81*, 27–35. [CrossRef]
30. Benhebal, H.; Chaib, M.; Leonard, A.; Lambert, S.D.; Crine, M. Photodegradation of Phenol and Benzoic Acid by Sol-Gel-Synthesized Alkali Metal-Doped ZnO. *Mater. Sci. Semicond. Process.* **2012**, *15*, 264–269. [CrossRef]

31. Léonard, G.L.-M.; Pàez, C.A.; Ramírez, A.E.; Mahy, J.G.; Heinrichs, B. Interactions between Zn2+ or ZnO with TiO_2 to Produce an Efficient Photocatalytic, Superhydrophilic and Aesthetic Glass. *J. Photochem. Photobiol. A Chem.* **2018**, *350*, 32–43. [CrossRef]
32. Mahy, J.G.; Lambert, S.D.; Léonard, G.L.M.; Zubiaur, A.; Olu, P.Y.; Mahmoud, A.; Boschini, F.; Heinrichs, B. Towards a Large Scale Aqueous Sol-Gel Synthesis of Doped TiO_2: Study of Various Metallic Dopings for the Photocatalytic Degradation of p-Nitrophenol. *J. Photochem. Photobiol. A Chem.* **2016**, *329*, 189–202. [CrossRef]
33. Geology, K.G. Geology, Petrology and Geochemistry of the Tertiary Bana Volcano-Plutonic Complex, West Cameroon, Central Africa. Ph.D. Thesis, Kobe University, Kobe, Japan, 2004.
34. Aboubakar, Y. *Etude Pédologique Du Terroir de Bana*; ORSTOM: Yaounde, Cameroon, 1974.
35. Bi Tra, T. *Etude Pédologique et Cartographique à L'échelle 1/50000 d'un Secteur de L'ouest-Cameroun (Région de Bafang)*; ORSTOM: Yaounde, Cameroon, 1980.
36. Benhebal, H.; Chaib, M.; Crine, M.; Leonard, A.; Lambert, S.D. Photocatalytic Decolorization of Gentian Violet with Na-Doped (SnO_2 and ZnO). *Chiang Mai J. Sci.* **2016**, *43*, 584–589.